Primary and Secondary Spray Breakup Modelling for Internal Combustion Engine Applications

Helge von Helldorff, Gerald J Micklow
Dept. Mechanical and Aerospace Engineering
Florida Institute of Technology
Melbourne, FL 32901, USA
hvonhelldorf2008@fit.edu

***Abstract*— A numerical investigation of primary and secondary breakup models was performed and compared to experimental literature data for both evaporating and non-evaporating cases. For this purpose, the Enhanced Taylor Analogy (ETAB) and Cascade Atomization Breakup (CAB) model were implemented in a three-dimensional compressible turbulent Navier-Stokes solver, KIVA 3V release 2, along with a comprehensive primary breakup model spanning all primary breakup regimes.**

It was found that the ETAB and CAB model performed in a nearly identically manner for the investigated cases but presented a significant improvement over the standard Taylor Analogy Breakup (TAB) model. The results of the primary breakup investigation suggest that even at conditions representative of the Diesel direct injection regime, primary breakup alone does not cause complete atomization of the spray. It is suggested that at the center of the spray, induced gas velocities due to momentum transfer from the spray, air entrainment, and particle-particle interactions reduce the relative velocity experienced by the center of the jet, suppressing primary breakup in this region and causing the production of larger droplets than in the outer spray region.

A hybrid primary breakup model to account for this bimodal behavior of the primary breakup is outlined in this paper. However, further experimental work is still needed to relate the introduced tuning constants to the spray conditions. With the estimated tuning constants utilized for this work, the results showed that the hybrid bimodal primary breakup model improves the prediction of spray penetration distance, spray angle and droplet size distribution.

Keywords*— *Primary Breakup, Secondary Breakup, Spray, CFD, KIVA, TAB model

I. INTRODUCTION

Spray modelling and droplet breakup represent one of the most crucial steps in the simulation of internal combustion engines, as the macroscopic spray parameters, such as spray penetration and spreading angle, along with the droplet characteristics, especially particle size distribution, determine the spatial distribution of gaseous combustible fuel within the cylinder. Failure to correctly predict particle size distributions will lead to an incorrect prediction of the evaporation and the resulting gaseous fuel distribution, which will then lead to errors in the combustion process calculation. The difficulty in fully describing and modelling a spray jet and breakup processes is due the large number of highly interconnected phenomena and mechanisms, such as primary and secondary breakup, heat transfer, evaporation, particle-particle interactions, aerodynamic forces, fluid forces (e.g. surface tension), droplet deformation etc. Failure to accurately describe any one of these mechanism may mask issues in the description of the other processes.

The particle breakup process is generally divided into two categories, i.e. the Primary Breakup and the Secondary Breakup. The primary breakup describes the transformation of the cylindrical liquid column emanating from the injector nozzle into distinct particles due to instabilities arising from the surface tension and forces introduced by the injector nozzle geometry, as well as due to aerodynamic effects. In most computational models that do not model the multiphase flow inside of the injector, such as Reynold's-Averaged-Navier-Stokes (RANS) calculations, the primary breakup is assumed to take place instantaneously at the nozzle exit and the liquid column is not explicitly simulated. Advanced simulation techniques such as Large Eddy Simulations (LES) and Direct Numerical Simulation (DNS) are generally required to explicitly model the liquid column. This simplifying assumption stands in contrast to the liquid core observed in real world sprays and depicted in Fig. 1.

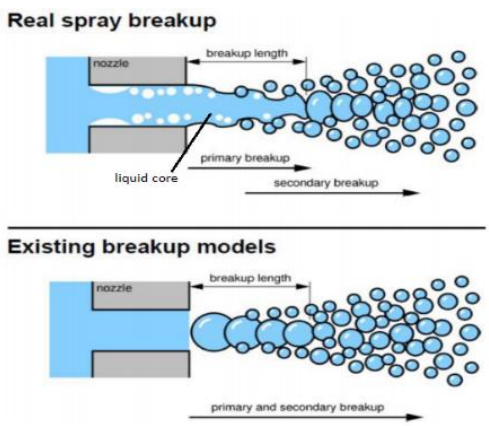

Fig. 1: primary breakup [1]

Occurring due to essentially the same processes as primary breakup, the secondary breakup describes the further breakup of the primary fuel particles into increasingly fine fuel mists. Both primary and secondary breakup occur in various modes, depending on the ambient and particle characteristics as described by the non-dimensional quantities, i.e. Reynold's Number, Weber Number and Ohnesorge Number. As Weber Number increases, both primary and secondary breakup produce larger numbers of smaller particles. High Weber Number sprays are therefore of particular interest for engine injection systems to ensure the quick and complete atomization and evaporation of the liquid fuel.

Air Esscentials – Exhibit 2010
Aroma 360 v. Air Esscentials
IPR No. 2025-00706

II. Primary Breakup

Many investigators simply set the initial drop radius equal to the radius of the nozzle exit [2]. This practice likely arose from the observation that the liquid core emanating from a nozzle is roughly the same diameter as the nozzle, a common assumption in the derivation of jet core dynamics.

Depending on the nozzle exit conditions, the primary breakup exhibits various breakup modes. At low injection velocity, the jet falls within the Rayleigh Regime or varicose breakup regime, which describes dripping flows. Instabilities arising from surface tension effects dominate this regime, which is characterized by large liquid column lengths and low velocity vectors perpendicular to the spray axis, resulting long primary breakup lengths and low spreading angles. The Rayleigh Regime is depicted in Fig. 2a).

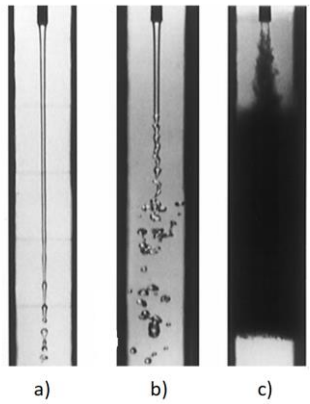

Fig. 2: Primary Breakup Modes [3] a) Rayleigh Regime b) Wind-Induced Regime c) Atomization Regime

As depicted in Fig. 3, the ligament first stretches until the diameter of the stretched ligament approaches zero, at which point breakup occurs and deformed particles are formed. Restoring surface tension forces then cause the particle to contract into a more spherical shape, which results in a particle that is larger than the originating nozzle and respective jet core ligament. Applying stability analysis according to Rayleigh [4] for the maximum growth rate of an axisymmetric disturbance and the corresponding wavelength and wave number leads to a spherical droplet diameter approximately 1.89 times larger than the nozzle diameter. However, Sunol et. al point out, that in experimental results, the droplets are often measured to be significantly larger (between two and three times the nozzle diameter) than this theoretical value, which they confirmed with high-speed videography to be due to coalescence shortly after the initial breakup event [5].

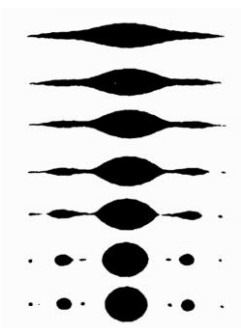

Fig. 3: Evolution of Ligament Stretching and Particle Formation with Satellite Particles [6]

Kerst et. al. propose the following relationship between droplet and nozzle diameter, which reverts to 1.88 d_{nozzle} if the Ohnesorge number is small [3].

$$r_{3,2} = 3r_n \left(\frac{3\pi}{\sqrt{2}}\right)^{\frac{1}{3}} (1 + 3\,Oh)^{\frac{1}{6}} \tag{1}$$

$$for\ 0.4\ or\ 1.2 + 3.4Oh^{0.9} \leq We_g < 13$$

However, there is very little (less than 5%) variation in droplet diameter [7]. As is commonly done, the variation in droplet diameter can thus often be neglected with minimal impact on accuracy.

The Wind-Induced Regime occurs at intermediate injection velocities and is often subdivided into the First Wind-Induced (FWI) or sinuous wave breakup regime, and the Second Wind-Induced (SWI) or wave-like breakup with air friction regime. The FWI regime is characterized by droplet diameters of the about same size as the nozzle exit. The common practice of setting the initial drop size equal to the nozzle is thus mostly applicable to this regime. In the FWI regime, surface tension is the main contributing source of instabilities and is opposed by inertia and air resistance, which results in surface waves and the production of ligaments, whose breakup if furthered by the air resistance.

In the SWI regime, as jet velocity and Weber number further increase, air resistance no longer acts as a damping factor but rather increases perturbations. Droplets in this regime are generally smaller than the nozzle diameter. Many empirical models exist to predict the droplet size in the wind induced regime, many of which are of similar format. Two such examples by Harmon [8]

$$d_{3,2} = 3330\ \left(d_n^{0.3}\mu_l^{0.07}\rho_l^{-0.648}\,\sigma^{-0.15}u^{-0.55}\mu_g^{0.78}\,\rho_g^{-0.052}\right) \tag{2}$$

and Wu et al. [9] [10] are presented here.

$$d_{3,2} = \frac{7d_n}{We_g}\left[\sqrt{\frac{x}{d_n}}\frac{We_g}{\sqrt{Re_l}}\right]^{0.87} \tag{3}$$

$$for\ 0.4\ or\ 13 \leq We_g < 40.3$$

Where x is the axial distance from the nozzle

The atomization regime, which occurs at high Weber numbers, is by far the least well understood regime. The liquid core dramatically changes in shape in the atomization regime, producing a conical structure rather than an elongated cylinder. Similar to stripping or catastrophic secondary breakup, relatively small droplets are abraded from the surface of the liquid cone through air friction effects, reducing the radius of the liquid cone with increasing distance from the nozzle, as shown in Fig. 4 A great difficulty in experimental investigations of primary atomization arises from the limitations of current measurement techniques. Optical techniques, such as Schlieren photography, shadowgraphy and video/photography can only visualize the external structure of the spray and measure penetration distance and spreading angle of the spray. The internal spray structure, including the liquid core and droplet sizes, is obscured by the fine atomized spray at the outer edge of the spray. Other

methods, such as X-Ray tomography can penetrate the optically dense outer spray, but many such techniques require a very small sampling volume and require only a single particle within that volume in order to determine droplet size. The near-injector region, however, is characterized by a high droplet number density.

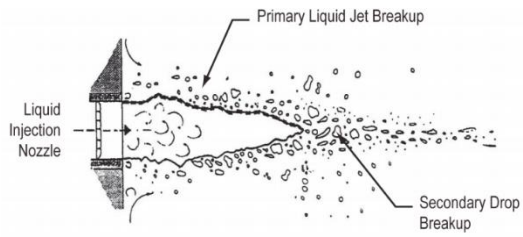

Fig. 4: Sketch of Primary and Secondary Liquid Jet Breakup [11]

For the atomization regime, one of many semi-empirical formulations for the Sauter mean diameter of the particle, SMD, may be utilized if the model does not inherently assume sphericity of particle. One such formulation was implemented in the KIVA code developed by Los Alamos National Labs [12] by Micklow et. al. [13], based on the experimental results by Elkotb [14].

$$\frac{d_{3,2}}{d_n} = 109.52\left(Re^{-0.183}We^{-0.442}C_d^{-0.442}\left(\frac{\rho_l}{\rho_a}\right)^{-0.05}\right)^{0.442}$$

$$for\ 40.3 \leq We_g \tag{4}$$

Fig. 5 depicts the various primary breakup regimes as a function of Reynold's Number and Ohnesorge Number, which is a dimensionless number relating the viscous forces to the inertial and surface tension forces. The figure also locates the two cases investigated in this paper, as well as the region of conditions most applicable to Diesel direct injection system on the Re-Oh plot. Reitz [15] further extended this Re-Oh plot to include the density ratio ρ_g/ρ_l, showing that increases in the density ratio increased breakup due to increased aerodynamic forces.

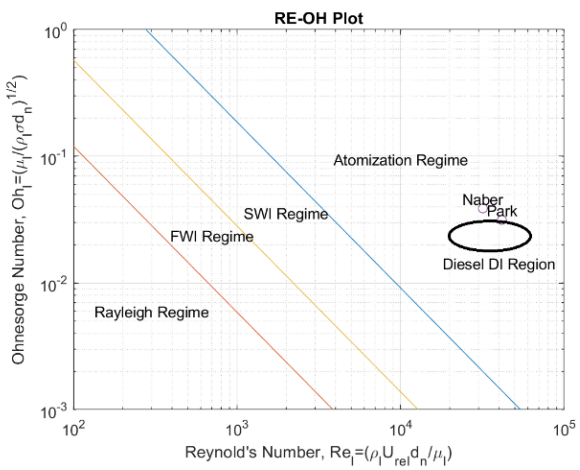

Fig. 5: Primary Breakup Regimes

III. SECONDARY BREAKUP

Secondary breakup models describe the processes by which existing droplets break up to form smaller particles. Like the primary breakup, several breakup modes exist for secondary breakup. As Weber number increases, aerodynamic effects increase and facilitate faster breakup resulting in the formation increasingly smaller droplets with increasing Weber number. The various secondary breakup modes are depicted in Fig.

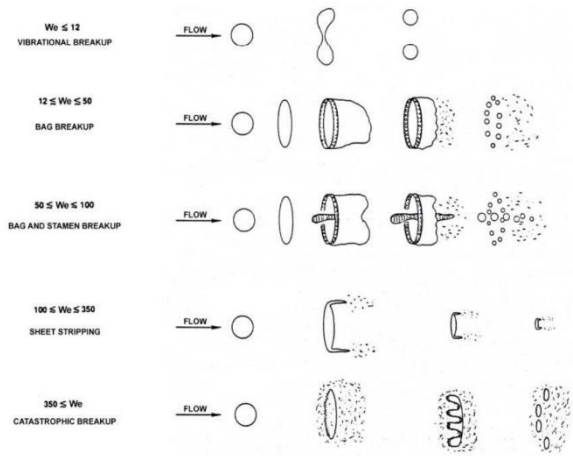

Fig. 6: Secondary Breakup Regimes by Weber Number [16]

A. TAB Model

The Taylor Analogy Breakup (TAB) model developed by O'Rourke and Amsden [17] is the native model in the KIVA code set. The TAB model draws the analogy between a mass spring system and the oscillation of the distorting liquid droplets.

Starting with the general equation for a damped forced oscillator

$$F - kx - d\frac{dx}{dt} = m\frac{d^2x}{dt^2} \tag{5}$$

with Taylor Analogy coefficients,

$$\frac{F}{m} = C_F\frac{\rho_g u^2}{\rho_l r} \tag{6a}$$

$$\frac{k}{m} = C_k\frac{\sigma}{\rho_l r^3} \tag{6b}$$

$$\frac{d}{m} = C_D\frac{\mu_l}{\rho_l r^2} \tag{6c}$$

where the constants,

$$C_k = 8, C_D = 5, C_F = \frac{1}{3}$$

are determined experimentally, the oscillator equation is non-dimensionalized assuming only a single mode of oscillation and setting $y = \frac{x}{C_b r}$.

$$\frac{d^2y}{dt^2} = \frac{C_F\rho_g u^2}{C_b\rho_l r^2} - \frac{C_k\sigma}{\rho_l r^3}y - \frac{C_D\mu_l}{\rho_l r^2}\frac{dy}{dt} \tag{7}$$

Further assuming underdamping of the droplets and constant relative velocities, the non-dimensional expression can be solved for the time rate of change of the distortion dy/dt, as well as for the distortion, y, where breakup occurs if y>1, The general solutions to these equations are

$$y(t) = We_c + e^{-\frac{t}{t_d}}\left[(y_0 - We_c)\cos(\omega t) + \frac{1}{\omega}\left(\frac{dy_0}{dt} + \frac{y_0 - We_c}{t_d}\right)\sin(\omega t)\right] \quad (8)$$

and

$$\frac{dy}{dt}(t) = \frac{We_c - y(t)}{t_d} + \omega e^{-t/t_d}\left\{\frac{1}{\omega}\left(\frac{y_0 - We_c}{t_d} + \frac{dy_0}{dt}\right)\cos(\omega t) - (y_0 - We_c)\sin(\omega t)\right\} \quad (9)$$

Where the Weber number and critical Weber number are defined as

$$We = \frac{\rho_g u^2 r}{\sigma} \quad (10a)$$

$$We_c = \frac{C_F}{C_k C_b} We = \frac{We}{12} \quad (10b)$$

Further, the initial distortion and initial time rate of change of distortion are assumed to be zero at the point of injection.

$$y_0 = y(0) \quad (11a)$$

$$\frac{dy_0}{dt} = \frac{dy}{dt}(0) \quad (11b)$$

The drop time constant and oscillation frequency are given by

$$t_d = \frac{2\rho_l r^2}{C_D \mu_l} \quad (12a)$$

$$\omega = \sqrt{\frac{C_k \sigma}{\rho_l r^3} - \frac{1}{t_d^2}} \quad (13b)$$

Solving the energy equation for the distorted child and parent droplets and equating the internal energy of the deformed parent droplet with the all child droplets allows for the calculation of the child droplet size. As the child droplet is assumed undeformed in the TAB model, the Sauter mean radius is equivalent to the drop radius.

$$r_{3,2,child} = \frac{r}{1 + \frac{8Ky^2}{20} + \frac{\rho_l r^3}{\sigma}\left(\frac{dy}{dt}\right)^2\left(\frac{6K-5}{120}\right)} \quad (14)$$

The number of child droplets is found through conservation of mass.

$$N^{n+1} = N^n\left(\frac{r^n}{r^{n+1}}\right)^3 \quad (15)$$

The child droplets further receive a velocity component normal to the parent droplet velocity, given by

$$v_{nor} = C_v C_b r\frac{dy}{dt} \quad where\ C_v \cong 1 \quad (16)$$

By finding the distortion amplitude, A, and assuming that the first oscillation period is not damped, the breakup time becomes the smallest possible root of an undamped version of equation (8) that is larger than the current time t^n.

$$A = \sqrt{(y^n - We_c)^2 + \left(\frac{\left(\frac{dy}{dt}\right)^n}{\omega}\right)^2} \quad (17)$$

$$We_c + Acos[\omega(t - t^n) + \Phi] = 1 \quad (18)$$

The breakup criterion can thus be defined as

$$We_c + A > 1 \quad (19)$$

If breakup does not occur during the time step, the droplet distortion and rate of distortion are updated as follows:

$$y^{n+1} = We_c + e^{-\frac{\Delta t}{t_d}}\left\{(y^n - We_c)\cos(\omega t) - \frac{1}{\omega}\left[\left(\frac{dy}{dt}\right)^n + \frac{y^n - We_c}{t_d}\right]\sin(\omega t\right\} \quad (20)$$

$$\left(\frac{dy}{dt}\right)^{n+1} = \frac{We_c - y^{n+1}}{t_d} + \omega e^{-\frac{\Delta t}{t_d}}\left\{\frac{1}{\omega}\left[\left(\frac{dy}{dn}\right)^n + \frac{y^n - We_c}{t_d}\right]\cos(\omega t) - (y^n - We_c)\sin(\omega t)\right\} \quad (21)$$

where

$$\cos(\Phi) = \frac{y^n - We^c}{A}$$

$$\sin(\Phi) = -\frac{\left(\frac{dy}{dt}\right)^n}{A\omega}$$

The TAB model has been surrounded by controversy. As Lee [18] points out, the original TAB paper by O'Rourke and Amsden included a typographical error in the $\sin(\omega t)$ part of the dy/dt equation (equation 9) , switching y0 and dy/dt(0) within the expression. However, it was verified that this error did not perpetuate into the KIVA source code, which was coded correctly. Lee et. al. further point out that the TAB model analysis of Ibrahim et. al. [19] omitted a factor of 0.5 in its presentation, leading to the TAB results as being incorrectly represented.

B. ETAB Model

The TAB model has been criticized for under-predicting droplet sizes and subsequently an entire class of breakup models has been developed based on a similar approach. The Enhanced Taylor Analogy Breakup (ETAB) model proposed by Tanner [20] marks the next step in the evolution of this model. The ETAB model utilizes largely the same algorithm, but with two notable modifications. The first difference is that in the ETAB model the production rate of child droplets is assumed to be proportional to the number of child droplets,

where the proportionality constant is dependent on the breakup regime.

$$\frac{dN}{dt}(t) = 3K_{br}N(t) \tag{22}$$

$$K_{br} = \begin{Bmatrix} k_1\omega \\ k_2\omega\sqrt{We} \end{Bmatrix} \; for \; \begin{matrix} We \le We_t \\ We > We_t \end{matrix} \tag{23}$$

$$where\ We_t = 80$$

$k_1 = 2/9 =$ ETAB Bag Breakup Factor

$k_2 = 2/9 =$ Stripping Breakup Factor

The uniform droplet size distribution is then determined by

$$\frac{r_{child}}{r_{parent}} = e^{-K_{br}t} \tag{24}$$

The child particles are initialized with zero distortion and zero rate of distortion. Similar to the original TAB model, the child particles assume a velocity component perpendicular to the parent particle

$$v_{normal} = A_c\frac{dx}{dt} \tag{25}$$

Where A_c is a constant describing how much of the axial parent velocity is converted to a normal velocity for the child particle and is determined from energy balance considerations.

$$A_c = \sqrt{3\left[1 - \frac{r_{parent}}{r_{child}} + \frac{5C_DWe}{72}\right]} * \frac{\omega}{\left(\frac{dy}{dt}\right)} \tag{26}$$

Where C_D is the drag coefficient and the distortion frequency, ω is given by

$$\omega = \sqrt{\frac{C_k\sigma}{\rho_l r_{parent}}} \tag{27}$$

However, unlike the standard TAB model, this normal velocity is now variable such that the normal velocity increases with increasing Weber number. The second major difference is that the ETAB model no longer assumes that the rate of droplet distortion dy/dt to be initially zero upon injection and breakup.

$$\frac{dy}{dt}(0) = \{1 - We_c[1 - \cos(\omega t_{bu})]\}\frac{\omega}{\sin(\omega t_{bu})} \tag{28}$$

$$t_{bu} = C\sqrt{\frac{\rho_p}{\rho_f}}\frac{d_{p,0}}{V_{P,0}} \quad where\ C = 5.5 \tag{29}$$

C. CAB Model

In a further iteration of the TAB model, Tanner introduced the Cascade Atomization and Drop Breakup (CAB) model [21]. The CAB model expands on the ETAB model, utilizing the exact same methodology, except for a refinement of the breakup constant used to obtain child droplet sizes.

$$K_{br} = \begin{Bmatrix} k_1\omega \\ k_2\omega\sqrt{We} \\ k_3\omega We^{3/4} \end{Bmatrix} for \begin{matrix} 5 < We < 80 \\ 80 < We < 350 \\ 350 < We \end{matrix} \tag{30}$$

$$k_2 = k_1\frac{\sqrt{1 - \frac{C_kC_b}{2C_fWe_t}}}{\operatorname{acos}\left(1 - \frac{C_kC_b}{C_fWe_t}\right)} \tag{30a}$$

$$k_3 = \frac{k_2}{We_{t2}^{\frac{1}{4}}} \tag{30b}$$

Where $k_1 = 0.05, We_t = 80, We_{t2} = 350$

D. MCAB Model

Finally, Kumzerova [22] further extended the applicability of the CAB model for very high and very low Weber Numbers by further optimizing the breakup constants, dubbing this extension the Modified Cascade Breakup (MCAB) Model.

E. Wave Model

Unlike the TAB model, the wave family of breakup models is derived from the stability analysis of cylindrical, viscous liquid jets into a gaseous, incompressible and inviscid gas. While the TAB models are limited to relatively low Weber numbers, the Wave model, developed by Reitz [23], is especially applicable to high speed injections with Weber numbers above 100. The Wave model assumes a liquid injection core, which is subjected to a relative velocity between the liquid and gas phase, resulting in Kevin-Helmholtz instabilities as a result of aerodynamic effects.

F. KH-RT Model

The KH-RT represents a hybrid model proposed by Beale and Reitz [24] represents a further evolution of the Wave model. As in the Wave model, the liquid core is subject to Kelvin-Helmholtz instability, describing the primary breakup of the jet. However, outside of the core, Rayleigh-Taylor breakup, which describes the instabilities on the droplet surface due to sudden acceleration of the ejected droplets into the freestream, becomes dominant.

G. SSD Model

All of the primary and secondary breakup models described above assume uniform initial droplet sizes due to the assumption of unimodal breakup. In real-world sprays, primary break up results in both major and satellite particles as shown in Fig. 3 and Fig. 7b). A much more rigorous, but also more computationally expensive approach to describe primary breakup with satellite formation was presented by Olesen [25].

For secondary breakup models, the Stochastic Secondary Droplet (SSD) model provides one alternative for modelling the multiple droplet size scales created by bimodal breakup and satellite formation [27]. The motivation for modelling these satellite particles has mainly been driven by the attempt to better predict gaseous fuel distributions especially near the injector nozzle by inclusion of these very small and quickly evaporating satellite droplets. However, Olesen found that satellite droplets only make up about 1.4% of the total spray

mass owing to their relatively much smaller size, despite occurring in similar numbers as the main particles [25].

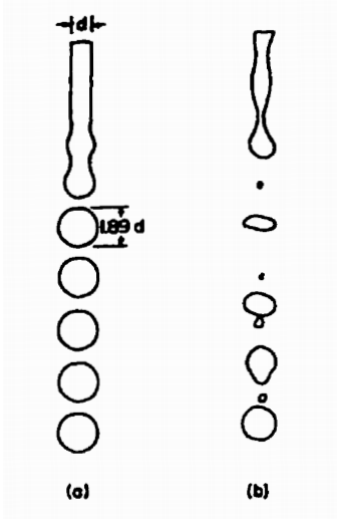

Fig. 7: a) idealized primary breakup b) real primary breakup with satellite droplet formation [26]

Chryssakis et. al. provide a useful in-depth summary of these and other secondary breakup models [28].

IV. Computational Model

For this paper, the ETAB and CAB secondary breakup models were implemented according to the equations outlined above and compared to the standard TAB model. Additionally, the effect of the primary breakup model on the results was investigated. To this end, a primary breakup model based on the relations by Kerst (eqn. 1) for the Rayleigh regime, and on Wu et. al. (eqn. 3) for the Wind-Induced Regime was implemented. For the atomization regime, three primary breakup models were investigated.

The model designated as PBU3, is a hybrid model of the Micklow/Elkotb model applied in the outer regions of the spray plume, and larger initial droplets at the center of the spray cone. This is accomplished by introducing a tuning constant, $0 \leq k_\Psi \leq 1$, which determines the ratio of the spray angle for the core, Ψ_c and total spray angle Ψ_{sp}. Additionally, the droplet radius is reduced as part of the liquid core has been abraded due to the atomization taking place at the outer edge of the liquid core. This reduction factor in this study is set equal to the same tuning constant, k_Ψ. Since the spray at the beginning of the injection event encounters a stagnant ambient gas and the velocity profile near the injector due to momentum transfer to the gas and air entrainment has not yet been established, the entire spray cone experiences conditions that promote atomization. For this reason, a time offset for the initiation of the primary breakup reduction, estimated as 0.1 ms for this study, is introduced. Therefore, the expression $d_{3,2} = 3k_\Psi d_n \quad for\ \Psi < \Psi_c$ is only utilized 0.1 ms after the initiation of the injection event. The factor 3 in these models is due to the definition of the Sauter mean radius for a spherical particle, which states that the average radius $\bar{r} = 1/3\ r_{3,2}$ [12]. PBU1 is thus an expression for setting the initial droplet radius equal to the injector nozzle radius.

TABLE I. Primary Breakup (PBU) Models

PBU1	$d_{3,2} = 3d_n$
PBU2	Micklow/Elkotb Model (eqn. 4)
PBU3	$\begin{cases} d_{3,2} = 3k_\Psi d_n & for\ \Psi < \Psi_c \\ Elkotb\ Model & for\ \Psi \geq \Psi_c \end{cases}$ $where\ \Psi_c = k_\Psi \Psi_{sp}$

The primary breakup regimes were determined by the critical Ohnesorge Number lines presented in the Re-Oh plot depicted in Fig. 5, which represent the following power law functions.

$$Reynold's\ Regime \leq Oh_{c1}$$

$$Oh_{c1} < Wind\ Induced\ Regime \leq Oh_{c2}$$

$$Oh_{c2} < Atomization\ Regime$$

Where

$$Oh_{c1} = 50 * Re^{-1.31} \tag{31a}$$

$$Oh_{c2} = 1587 * Re^{-1.31} \tag{31b}$$

For this study, the results were compared to two literature cases. The first case is a high ambient pressure, high ambient temperature, evaporating spray, presented by Naber and Siebers [29] which provides additional documentation and materials on the Engine Combustion Network (ECN) website [30]. All simulations for this case were performed with a square mesh of 8x8x10.9 cm with 40x40x100 vertices and all solid wall boundary conditions. The test conditions are outlined in Table II and Table III below.

TABLE II. Gas Composition for Evaporative Case (Naber & Siebers)

Species	%Vol	%Mass
O2	0	0
N2	90.33	88.37
CO2	6.11	9.39
H2O	3.56	2.24

TABLE III. Simulated Experimental Conditions for Evaporative Case (Naber&Siebers)

ΔP	139 MPa
P_{amb}	8.304 MPa
T_{amb}	1000 K
ρ_{amb}	28.6 kg/m^3
Δt_{inj}	3.6 ms
T_{inj}	300 K
d_n	0.198 mm
V_{inj}	308 m/s
$\dot{m}_{inj}$	8 g/s
d_{vol}	109 mm

The second case represents a low ambient pressure, low ambient temperature, non-evaporating case in ambient air by Lee and Park [31].

The mesh for this case was a square mesh of 8x8x10 cm and 40x40x100 vertices, with an open boundary condition at the side opposite the injector. In both cases the mesh size was chosen to recreate the experimental distance between the injector nozzle and the opposing wall, while avoiding wall effects and interactions on the mesh sides.

TABLE IV. TEST CONDITIONS FOR NON-EVAPORATIVE CASE (LEE & PARK)

P_{amb}	1 atm
T_{amb}	300 K
P_{inj}	80 MPa
Δt_{inj}	1.4 ms
T_{inj}	300 K
d_n	0.3 mm
$\dot{m}_{inj}$	14.379 g/s
V_{inj}	266.24 m/s
Ψ_{sp}	15.1 deg

Both cases used Diesel Fuel 2 (DF2) as the injection medium and square injection pulses.

V. RESULTS

Fig. 12 depicts the spray evolution with time of the evaporating jet simulating the experimental conditions by Naber and Siebers. All models displayed here use the same primary breakup mechanism, PBU1, setting the initial droplet size equal to the injector nozzle diameter. The experimental results are shown in the first column. It must be stressed here that Naber and Siebers explicitly state that in these experimental pictures full extinction of background light is associated with the extend of the liquid spray, while Schlieren effects or partial extinction of the background light is mainly associated with gaseous fuel and temperature gradients. Unfortunately, this makes the analysis of these pictures rather subjective, as the exact extend of the liquid spray is not readily determinable. For higher resolution pictures of the experiment, the reader is referred to the evaporating case of the "Evaporating vs. Non-Evaporating" study by Naber and Siebers available through the Engine Combustion Network (ECN) [30]. It should further be noted that each particle marker in the simulations depicts a parcel representing multiple droplets.

The ETAB and CAB model (second and third column of Fig. 12) perform with no discernable differences with respect to spray penetration and spray angle. In both cases, the spray characteristics appear well matched for the first 0.7 ms. After 1.26 ms, the spray angle notably exceeds the experimental results, and after 2.24 ms, the spray penetration of the models markedly enters the Schlieren region of the experimental photographs.

The TAB (Fig. 12 column 4) model does not perform well under the modelled high ambient density conditions. Overprediction of breakup is the well-established main criticism on the performance of the standard TAB model. In the presented case, the high ambient density facilitates breakup and the high temperature evaporates the resulting small droplets nearly instantaneously such that a liquid spray plume is never developed.

For comparison, the last column of Fig. 12 depicts the same simulation without secondary breakup mechanism, such that droplet size reductions are mainly due to evaporation. As expected, the jet penetration is overpredicted at all time steps. The spray angle, however, is well-matched, as no velocity gradients perpendicular to the droplet path are introduced by breakup processes in this case.

The non-evaporating case depicted in Fig. 14 shows similar results to the evaporating case. Both, the ETAB and CAB model again with no discernable differences, but show slight over-predictions in spray penetration at 0.2 ms and 1.4 ms. While the TAB model performs significantly better in this case, spray penetration is notably underpredicted, especially at the late stages of the spray development. Additionally, the low parcel density suggests that many droplets reached a cutoff size, at which the KIVA code converts these exceedingly small particles to the gas phase. Again, by inhibiting secondary breakup, the penetration distance is significantly overpredicted.

These results suggest that CAB and ETAB model performance is significantly superior to the TAB model. However, the penetration distance and spray angle over prediction further suggest that the primary breakup model PBU1 overestimates the initial droplet size. This is further supported by the large droplet sizes relative to the nozzle diameter, especially near the spray tip, as depicted by the colorbars in these figures. As shown in Fig. 5 both cases are clearly located within the primary atomization regime. PBU1, however, is mostly applicable to the wind-induced regime. PBU2 (Micklow/Elkotb model) on the other hand is a primary atomization regime model.

The second and third columns of Fig. 13 and Fig. 15 compare the performance of primary breakup models PBU1 and PBU2 in conjunction with the CAB secondary breakup model. While PBU1 matches the initial plume formation relatively well but over predicts penetration and spray angle as the spray plume evolves, PBU2 significantly under-predicts spray penetration and spray angle in every plume development stage. These results led to the development of the hybrid model PBU3, depicted in the fourth column of Fig. 13 and Fig. 15. As already noted by Reitz [15], the primary breakup regime limits depicted in Fig. 5 demark the onset of e.g. the atomization regime transition. However, the Micklow/Elkotb model (PBU2) assumes full atomization of the spray through primary breakup alone. It is proposed that a significant transition regime between the wind-induced regime and the atomization regime exists, in which the outside of the spray cone experiences atomization, while the inner spray cone remains within the wind breakup regime, such that the extent to which atomization occurs increases with increasing Weber number. This bimodal behavior is due to the high aerodynamic shear forces at the outside of the jet causing atomization, while momentum transfer, air entrainment and particle-particle interactions significantly reduce the relative velocity between the gaseous medium and the droplets at the center of the spray cone. Thus, primary breakup is inhibited at the center of the jet. However, the resolution of most practical RANS simulation is too coarse to fully resolve these velocity gradients and particle interactions, requiring an empirical formulation to determine the ratio of spray within the atomization and wind-induced regime respectively. As a first starting point, the PBU3 model utilizes a tuning constant, k_Φ, to determine the ratio large particle core spray angle to the full spray angle, as well as the initial droplet size at the jet center. For comparability, all PBU3 simulations presented here are performed with k_Φ set to 0.5, meaning that the droplets originating from within one half of the full spray angle are assumed to be in the wind-induced regime.

Column 4 of Fig. 13 and Fig. 15 show an improvement of the spray angle compared to the PBU1 and PBU2 CAB simulations, as well as an improvement of the spray penetration prediction for the well-developed spray. However, the spray penetration is still notably underpredicted at the early spray development stage.

It should be emphasized here that the initial droplet size at the core region, set to equal the nozzle radius, is only utilized to demonstrate the new bimodal primary breakup approach and likely represents a significant over-estimation of the droplet size. Experimental research into the radial droplet size distribution is required to complete and validate the PBU3 bimodal approach. Similarly, the k_{Φ}value of 0.5 was chosen somewhat arbitrarily to fit the results presented here. Again, experimental data is still needed to determine an empirical relationship for this tuning constant as a function of spray conditions, as well as the initial time offset for the primary breakup reduction.

Fig. 13 further depicts the performance of the primary breakup models without secondary breakup for comparison. Finally, Fig. 15 presents the PBU2/TAB case for comparison, which again underpredicts spray penetration and spray angle due to extreme droplet breakup. The low spray angle and low parcel density, along with the small droplet radius depicted by the marker coloring support the conclusion that breakup is overpredicted.

The macroscopic spray characteristics, such as spray penetration and spray angle provide only a partial picture. Additional insight can be gained by examining the droplet size distributions. Fig. 8 depicts the experimental axial droplet size distribution by Lee and Park, along with the parcel sizes predicted by the PBU3/TAB model. This figure demonstrates the extend of droplet size under-prediction by the TAB model, as most of the parcels are less than 1 micrometer in diameter, i.e. more than one order of magnitude less than the experimental average, and no parcels are predicted to be larger than the experimental average.

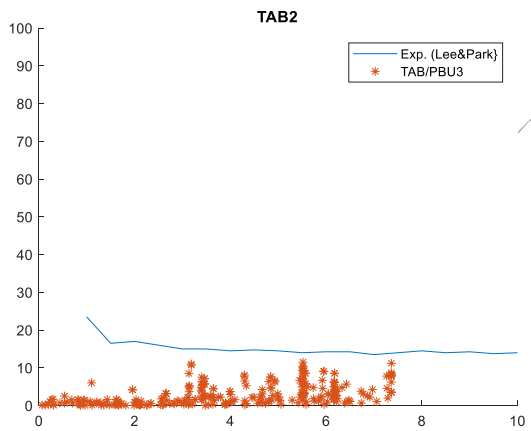

Fig. 8: Droplet Size Distribution PBU3/TAB

Fig. 9 depicts the same information for the PBU3/CAB model, with Fig. 10 providing a magnification of the lower diameter range. In this case, the majority of parcels is in the 0 to 10 micrometer range, but are significantly more evenly distributed across this range than in the TAB model. A number of droplets are predicted at significantly larger diameters. These mainly correspond to droplets originating from the core region of the PBU3 model. The large predicted diameter of these parcels is partially due to coalescence through collision events, as well as overpredictions from the Gaussian distribution applied to the initial size distribution by KIVA [12]. These results further suggest that the initial droplet diameter in the core region, set to one half (in the presented case) of the nozzle diameter in the PBU3 model, represents an over-estimation and needs to be refined in future research based on experimental findings.

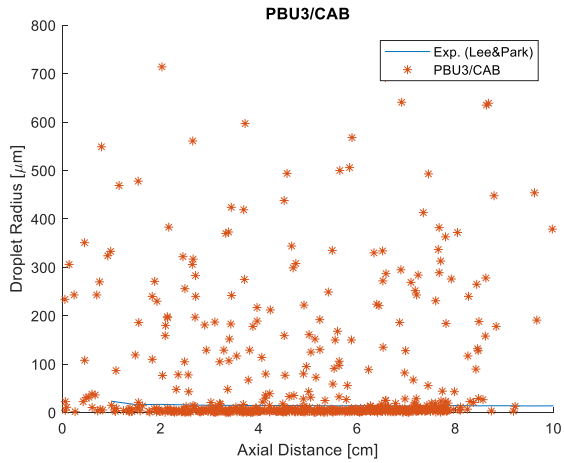

Fig. 9: Droplet Size Distribution PBU3/CAB

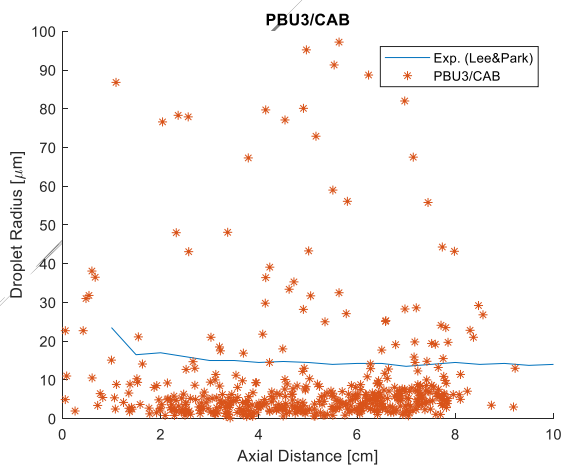

Fig. 10: Droplet Size Distribution PBU3/CAB (magnified)

Fig. 11 shows that by neglecting to account for the reduced primary breakup at the core, the average droplet size is under-predicted, especially as distance to the nozzle increases, as nearly all parcels are smaller than the average droplet size measured by Lee and Park. This further suggests that the jet does not completely atomize through the primary breakup alone and that primary breakup is in fact reduced at the center of the jet.

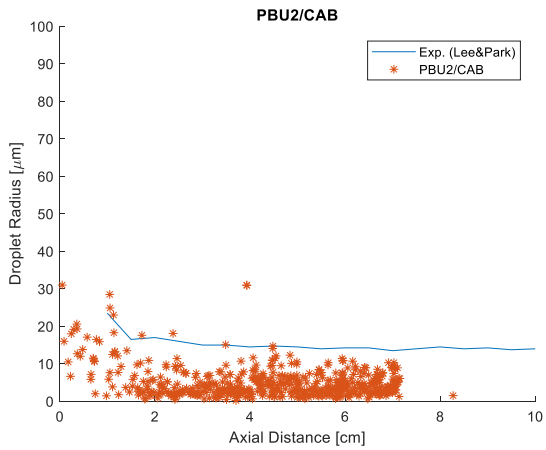

Fig. 11: Droplet Size Distribution PBU2/CAB

VI. Conclusions

The Enhanced Taylor Analogy Breakup (ETAB) and Model Cascade Atomization Breakup (CAB) were implemented in KIVA 3V release 2 and results using these models were compared to the standard TAB model as well as two literature cases representing both evaporating and non-evaporating conditions within the atomization regime representative of Diesel direct injection conditions.

It was found that under the investigated conditions the ETAB and CAB model performed in a similar fashion, but represented a significant improvement compared to the TAB model with respect to predicting the spray penetration, spreading angle, droplet size and overall spray plume shape.

A comprehensive primary breakup model was implemented covering all primary breakup regimes. For the atomization regime a bimodal primary breakup mechanism was introduced to account for the reduced primary breakup due to the induced gas velocity, air entrainment and particle-particle interactions at the center of jet.

This bimodal approach showed improved performance of the model with respect to penetration distance, spray angle and droplet size, compared to the primary breakup model that assumes full atomization by primary breakup alone.

VII. Future Work

It should be noted that the bimodal primary breakup approach introduced here in its current stage is not meant to be seen as complete. Experimental data is still needed to describe the tuning constant used to determine the primary breakup reduction and droplet size at the spray center as a function of spray characteristics.

Additional factors not addressed by this paper that still need to be addressed in further research include the Gaussian size distribution's tendency to produce a small number of excessively large particles, as well the droplet drag coefficient. The current drag coefficient expression does not account for particle-particle interactions, such as drafting. An empirical reduction of the drag coefficient based and droplet number density and size distribution to account for these effects especially in the dense spray region near the injector is expected to improve the underprediction of spray penetration in the early spray development stage.

VIII. Nomenclature

A. Variables and constants

$$Re_l = Reynold's\ Number = \frac{u_{rel} d_{smr} \rho_l}{\mu_l}$$

$$We_l = Weber\ Number = \frac{u_{rel}^2 d_d \rho_l}{\sigma} = \frac{inertial\ /\ aerodyn.\ forces}{surface\ tension}$$

$$Oh = Ohnesorge\ Number = \frac{\sqrt{We_l}}{Re_l}$$

$\rho = density$

$\mu = viscosity$

$\sigma = surface\ tension$

$\Psi_{sp} = total\ spray\ angle$

$\Psi = spray\ angle\ of\ individual\ parcel$

$\omega = distortion\ wave\ frequency$

$A = distortion\ amplitude$

$A_c = ratio\ of\ axial\ to\ normal\ velocity$

$C = constant\ (various)$

$C_b = critical\ amplitude\ coefficent = 0.5$

$C_d = discharge\ coefficient$

$C_D = damping\ coefficent = 5.0$

$C_F = external\ force\ coefficent = 1/3$

$C_k = restoring\ force\ coefficent\ = 8.0$

$C_v = new\ droplet\ velocity\ factor$

$d = diameter$

$F = force$

$K = energy\ ratio\ factor\ = 10/3$

$m = mass$

$N = number\ of\ droplets$

$P = Pressure$

$r = radius$

$T = Temperature$

$dt = time\ step = t_2 - t_1$

$t = time$

$t_d = time\ constant$

$u = velocity$

$V_{inj} = injection\ velocity\ at\ nozzle$

$v_{nor} = droplet\ normal\ velocity\ compenent$

$x = distance$

$y = distortion$

B. Sub/Superscripts

$0 = initial\ (t = 0)$

$3{,}2 = Sauter\ Mean\ (radius\ or\ diameter)$

$c = critical$

$d = droplet$

$g = amb = ambient\ gas$

$inj = injection, at\ the\ nozzle$

$l = liquid$

$n(subscript) = nozzle$

$n(superscript) = current\ time\ step$

$rel = relative$

VI. REFERENCES

[1] [1] D. Nsikane, K. Mustafa, A. Ward, R. Morgan, D. Mason and M. Heikal, "Statistical Approach on Visualizing Multi-Variable Interactions," SAE Int. J. Engines, vol. 10, no. 5, pp. 2461-2477, 2017.

[2] R. Reitz, "Modeling Atomization Processes in High-Pressure Vaporizing Sprays," Atomization and Spray Technology, vol. 3, pp. 309-337, 1987.

[3] A. Kerst, B. Judat and E. Schlunder, "Flow regimes of free jets and falling films at high ambient pressure," Chemical Engineering Science, vol. 55, pp. 4189-4208, 2000.

[4] L. Rayleigh, "On the Stability of Certain Fluid Motions," Proceedings of the London Mathematical Society, vol. 1, no. 1, p. 57–72, 1879.

[5] F. Suñol and R. González-Cinca, "Liquid jet breakup and subsequent droplet dynamics under normal gravity and in microgravity conditions," Physics of Fluids, vol. 27, 2015.

[6] M. Tjahjadi, J. Ottino and H. Stone, "Satellite and Subsatellite Formation in Capillary Breakup," Journal of Fluid Mechanics, vol. 243, pp. 297-317, 1992.

[7] H. Teng, C. Kinoshita and S. Masutani, "Prediction of droplet size from the breakup," International Journal of Multiphase Flow, vol. 21, no. 1, pp. 129-136, 1995.

[8] D. Harmon, "Drop Sizes from Low Speed Jets," Journal of the Franklin Institute, vol. 259, no. 5, pp. 519-522. , 1955.

[9] P. Wu, L. Tseng and G. Faeth, "Primary breakup in gas/liquid mixing layers for turbulent liquids," Atomization and Sprays, vol. 2, pp. 295-317, 1992.

[10] P. Wu and G. Faeth, "Onset and end of drop formation along the surface of turbulent liquid jets in still gases," Physics of Fluids , vol. 7, no. 11, pp. 2915-2917, 1995.

[11] H. Trinh, "Modeling of Turbulence Effect on Liquid Jet Atomization," NASA/TM—2007–215189, 2007.

[12] A. Amsden, P. O'Rourke and T. Butler, "KIVA-II: A Computer Program for Chemically Reactive Flows with Sprays," Los Alamos Report LA-11560-MS, 1989.

[13] G. J. Micklow, K. Ankem and T. Abdel-Salam, "A Comprehensive Fuel Spray Model for High Pressure Fuel Injectors," in ASME Turbo Expo 2008: Power for Land, Sea, and Air, Berlin, Germany, 2008.

[14] M. Elkotb, "Fuel atomization for spray modelling," Progress in Energy and Combustion Science, vol. 8, no. 1, pp. 61-91, 1982.

[15] R. Reitz, "Atomization and other breakup regimes of a liquid jet," Dissertation Princeton University, 1978.

[16] M. Pilch and C. Erdmann, "Use of breakup time data and velocity history data to predict the maximum size of stable fragments," International Journal of Multiphase Flow, vol. 13, no. 6, pp. 741-757, 1987.

[17] P. O'Rourke and A. Amsden, "The TAB Method for Numerical Calculations of SPray Droplet Breakup," in International Fuels and Lubricants Meeting and Exposition, Toronto, 1987.

[18] M. W. Lee, J. J. Park, M. M. Farid and S. S. Yoon, "Comparison and correction of the drop breakup models for stochastic dilute spray flow," Applied Mathematical Modelling, vol. 36, pp. 4512-4520, 2012.

[19] E. A. Ibrahim, H. Q. Yang and A. J. Przekwas, "Modeling of spray droplets deformation and breakup," Journal of Propulsion Power, vol. 9, pp. 651-654, 1993.

[20] F. X. Tanner, "Liquid Jet Atomization and Droplet Breakup Modeling of Non-Evaporating Diesel Fuel Sprays," SAE Transactions, vol. 106, pp. 127-140, 1997.

[21] F. Tanner, "Development and Validation of a Cascade Atomization and Drop Breakup Model for High Velocity Dense Sprays," Atomization and Sprays, vol. 14, pp. 211-242, 2004.

[22] E. Kumzerova and T. Esch, "Extension And Validation Of The Cab Droplet Breakup Model To A Wide Weber Number Range," in ILASS, Como Lake, 2008.

[23] R. D. Reitz, "Modeling atomization processes in high-pressure vaporizing sprays," Atomization and Spray Technology, vol. 3, pp. 309-337, 1987.

[24] J. C. Beale and R. D. Reitz, "Modeling Spray Atomization with the Kelvin-Helmholtz/Rayleigh-Taylor Hybrid Model," Atomization and Sprays, vol. 9, p. 623–650, 1999.

[25] M. Olesen, "Predicition of drop-size distribution based on ligmanet breakup," Dissertation Queen's Universtiy at Kingston, 1997.

[26] A. Lefebvre, Atomization of Sprays, New York: Hemisphere, 1989.

[27] S. Apte, M. Gorokhovski and P. Moin, "LES of Atomizing Spray with Stochastic Modeling of Secondary Breakup," International Journal of Multiphase Flow, vol. 29, p. 1503 –1522, 2003.

[28] C. Chryssakis, D. Assanis and F. X. Tanner, "Atomization Models," Handbook of Atomization and Sprays, 2011.

[29] J. Naber and D. Siebers, "Effects of Gas Density and Vaporization on Penetration and Dispersion of Diesel Sprays," SAE Technical Paper 960034, 1996.

[30] Engine Combustion Network. [Online]. Available: https://ecn.sandia.gov/tutorials/diesel-spray/vaporizing-and-non-vaporizing/.

[31] C. S. Lee and S. W. Park, "An experimental and numerical study on fuel atomization characteristics of high-pressure diesel injection sprays," Fuel, vol. 81, pp. 2417-2423, 2002.

IX. Appendix

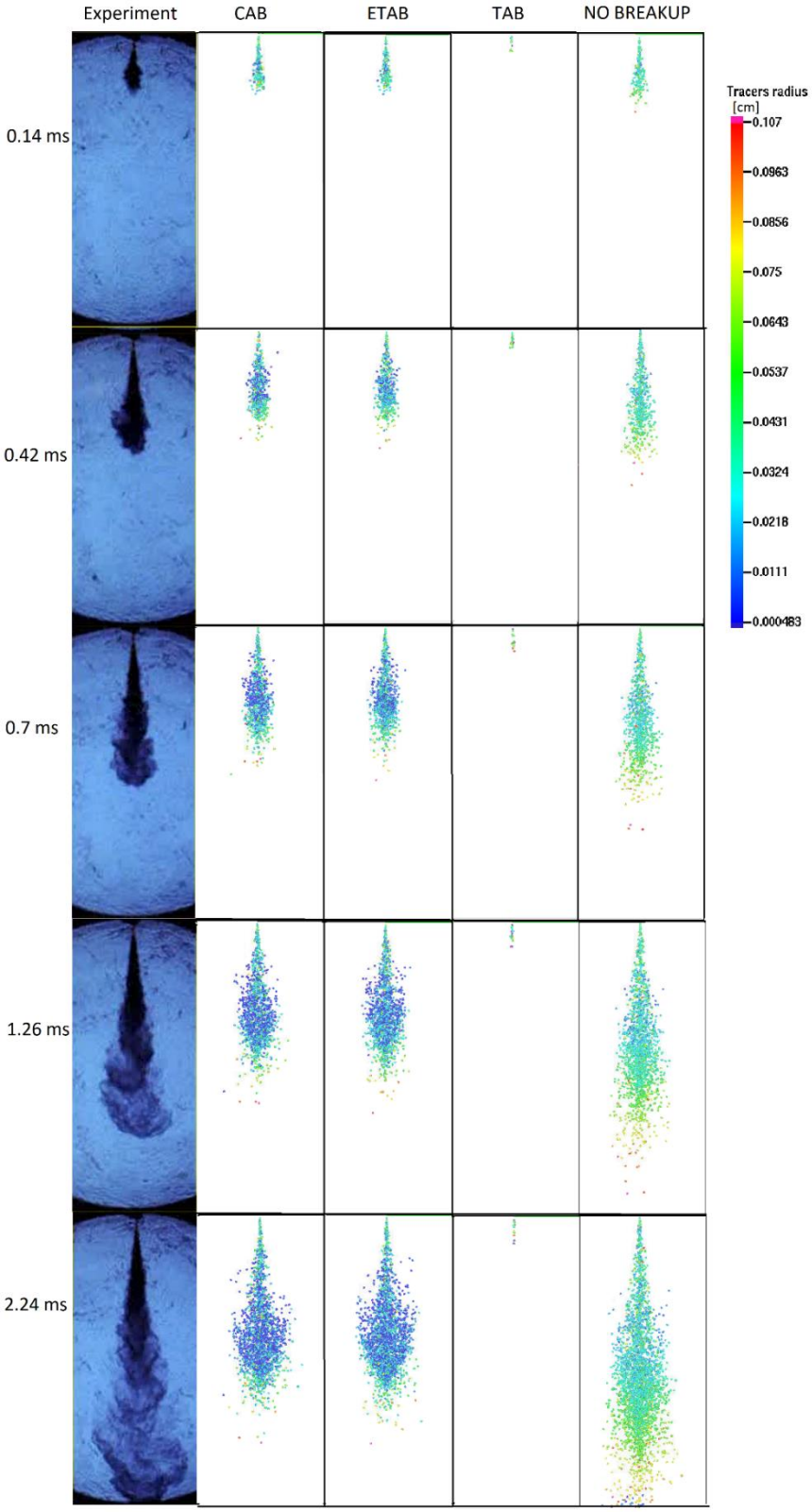

Fig. 12: Secondary Breakup Models for Evaporating Case (Naber & Siebers) (all cases utilizing PBU1)

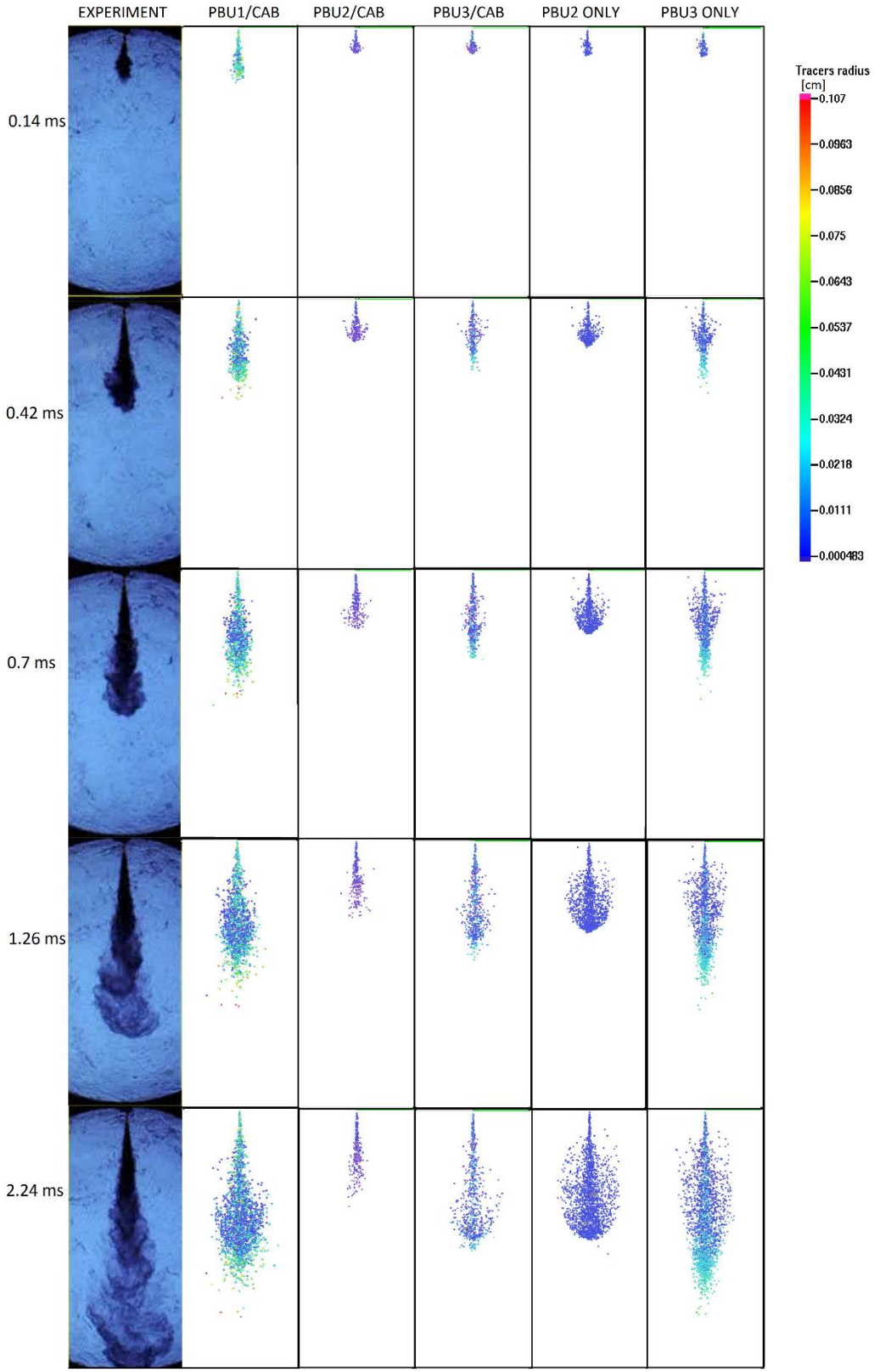

Fig. 13: Primary Breakup Models for Evaporating Case (Naber & Siebers)

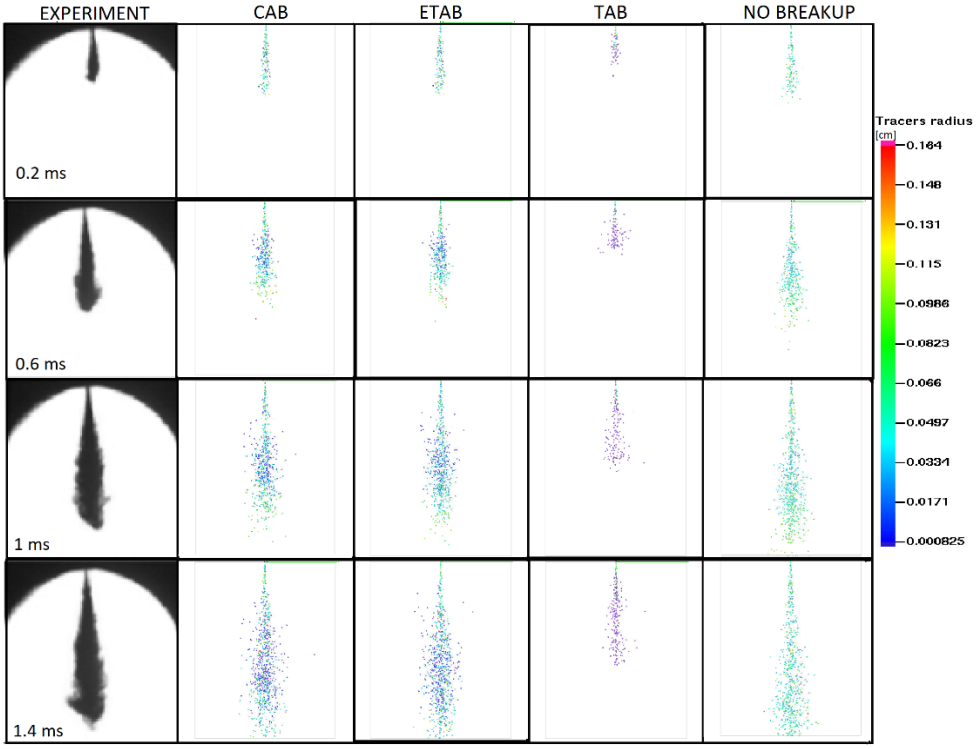

Fig. 14: Secondary Breakup Models for Non-Evaporating Case (Lee & Park) (all cases utilizing PBU1)

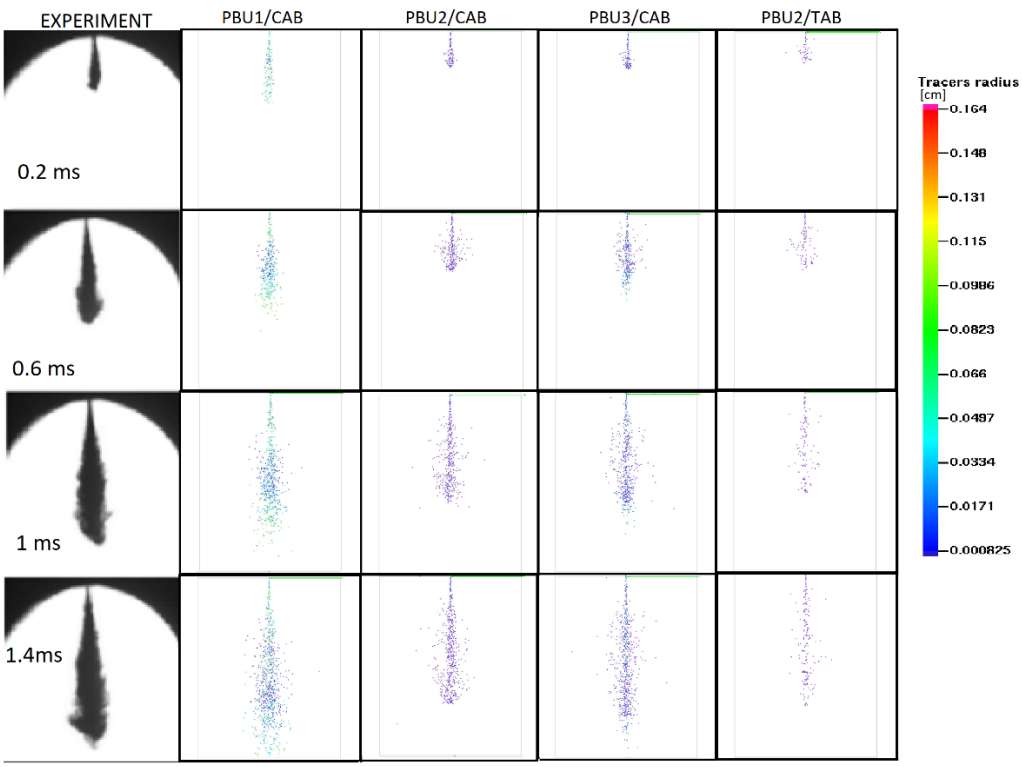

Fig. 15: Primary Breakup Models for Non-Evaporating Case (Lee & Park)